SEECCM III
3rd South-East European Conference on Computational Mechanics-
an ECCOMAS and IACM Special Interest Conference
M. Papadrakakis, M. Kojic, I. Tuncer (eds.)
Kos Island, Greece, 12–14 June 2013

FAST DETECTION OF CHAOTIC OR REGULAR BEHAVIOR OF DOUBLE PENDULUM SYSTEM: APPLICATION OF THE FAST NORM VECTOR INDICATOR METHOD

Dumitru N. Deleanu

Maritime University of Constanta
104, Mircea cel Batran street, Constanta, Romania
dumitrudeleanu@yahoo.com

Keywords: Double Pendulum Dynamics, Indicators of Regularity and Chaos.

Abstract. *It is well known that for non-linear Hamiltonian systems there exist ordered regions with quasi-periodic orbits and regions with chaotic orbits. Usually, these regions are distributed in the phase space in very complicated ways, which often makes it very difficult to distinguish between them, especially when we are dealing with many degrees of freedom. Recently, a new, very fast and easy to compute indicator of the chaotic or ordered nature of orbits has been introduced by Zotos (2012), the so-called "Fast Norm Vector Indicator (FNVI)". Using the double pendulum system, in the paper we present a detailed numerical study comporting the advantages and the drawbacks of the FNVI to those of the Smaller Alignment Index (SALI), a reliable indicator of chaos and order in Hamiltonian systems. Our effort was focused both on the traditional behavior of the FNVI for regular and fully developed chaos but on the "sticky" orbits and on the quantitative criterion proposed by Zotos, too.*

1 INTRODUCTION

Chaos theory is a scientific discipline that focuses on the study of non-linear dynamical systems that are highly sensitive to initial conditions. Today, chaos theory is applied in many other scientific disciplines: mathematics, biology, computer science, economics, engineering, finance, politics, population dynamics and so on.

Appearance of chaos has been identified through various methods/ indicators in the past. We mention here only the well-known tools: the time series method, phase-space method, Lyapunov exponents, bifurcation diagram, Kolmogorov entropy and the Poincare section of surface [1-4]. Some recent tools seem to be more efficient for distinguishing between chaotic or regular orbits, especially in higher order dynamical systems. First Lyapunov Indicator (FLI) was introduced by Froeschle et al. [5] and applied to the structure of a steroidal belt. Saha et al. applied the FLI to study certain discrete maps like Tinkerbell map, Ikeda map and Duffing map [6]. Other maps (Gaussian map, Delayed logistic map) were studied by Deleanu [7]. Fouchard et al. introduced a variant of FLI, the Orthogonal Fast Lyapunov Indicator [8]. Smaller Alignment Index (SALI) was proposed by Skokos [9] and has been successfully applied to some symplectic maps or Hamiltonian flows. A generalized version, the Generalized Alignment Index (GALI) was tested in 2007 [10]. A qualitative tool, the Dynamic Lyapunov Indicator (DLI) was introduced by Saha et al. and applied to various maps [11, 12]. The record could continue to include Spectral Distance (SD), the Dynamical Spectras of Stretching Numbers [13], the Relative Lyapunov Indicator [14], the 0-1 test [15], the Asymmetry Coefficients [16] or Dynamical Spectras of Helicity or Twist Angles [17].

Very recently, a simple, fast and efficient method called Fast Norm Vector Indicator (FNVI) was introduced by Zotos in order to distinguish rapidly and with certainty between ordered and chaotic motions in Hamiltonian systems. The method was applied in the case of a 2-Dof and a 3-Dof Hamiltonians [18].

We have thought that other numerical studies are necessary for a better understanding of the behavior of this indicator, especially in the transition zones between ordered regions and chaotic seas. In the same time, we have considered that some corrections must be made on the indicator proposed by the author. To this purpose, we present in the paper a detailed numerical study on the FNVI method using as a guide the double pendulum system.

The organization of the rest of the paper is as follows. Section 2 contains the details of the FNVI and SALI methods. In Section 3 we derive the Hamiltonian's equations of motion for the double pendulum system. All the calculations and numerical results are presented in Section 4. Finally, some concluding remarks are given in Section 5.

2 INDICATORS OF CHAOS AND ORDER: SALI AND FNVI

Let us consider an autonomous Hamiltonian system of N degrees of freedom (N dof), described by the Hamiltonian $H(q_1, q_2,..., q_N, p_1, p_2,..., p_N)$, where q_i and $p_i, i = 1, 2,..., N$ are the generalized coordinates and conjugate moments respectively.

An orbit in the $2N$ – dimensional phase space of this system is defined by the vector $\mathbf{x}(t) = (q_1(t), q_2(t),..., q_N(t), p_1(t), p_2(t),..., p_N(t))$, with $x_i = q_i, x_{i+N} = p_i, i = 1, 2,..., N$. The time evolution of this orbit is governed by Hamilton's equations of motion

$$\frac{dq_i}{dt} = \frac{\partial H}{\partial p_i} \quad , \quad \frac{dp_i}{dt} = -\frac{\partial H}{\partial q_i}, i = 1, 2,..., N \tag{1}$$

while the time evolution of the deviation vector $\xi(0) = (dx_1(0), dx_2(0),..., dx_{2N}(0))$ from the

$\mathbf{x}(t)$ solution of Eqs. (1) is given by the variational equations

$$J \cdot \dot{\xi}' = DH \cdot \xi' \tag{2}$$

where (‘) denotes the transpose matrix and matrices *J* and *DH* are defined by

$$J = \begin{pmatrix} O_N & -I_N \\ I_N & O_N \end{pmatrix} \quad , \quad DH_{i,j} = \frac{\partial^2 H}{\partial x_i \, \partial x_j}, i, \; j = 1, 2, ..., 2N \tag{3}$$

2.1 Smaller Alignment Index (*SALI*)

To define the *SALI* for an orbit with initial conditions $\mathbf{x}(0) = (x_1(0), x_2(0), ..., x_{2N}(0))$ we must follow the evolution in time of two initial deviation vectors $\xi_1(0)$ and $\xi_2(0)$. At every time step we normalize each vector to 1 and define the parallel alignment index $d_-(t) = \left\| \frac{\xi_1(t)}{\|\xi_1(t)\|} - \frac{\xi_2(t)}{\|\xi_2(t)\|} \right\|$ and the anti-parallel alignment index $d_+(t) = \left\| \frac{\xi_1(t)}{\|\xi_1(t)\|} + \frac{\xi_2(t)}{\|\xi_2(t)\|} \right\|$. Here, $\|\cdot\|$ denotes the Euclidean norm of a vector.

The *SALI* is defined as the minimum value of the above alignment indices at any point in time

$$SALI(t) = \min(d_-(t), d_+(t)) \tag{4}$$

Skokos proves that the two deviation vectors tends to coincide or become opposite for chaotic orbits, i.e. the *SALI* tends to zero. For ordered orbits, which lie on a torus, the two deviation vectors eventually become tangent to the torus but in general converge to different directions, so the *SALI* does not tend to zero. Its values fluctuate around a positive value [9].

2.2 The Fast Norm Vector Indicator (*FNVI*)

Let t^* be the predefined time step of the numerical integration of the system (1) and $[0, T]$ the interval of integration. The *FNVI* at the time moment $t = k\,t^*$ is defined as

$$FNVI(t) = \frac{1}{t} \left| \frac{\|\mathbf{x}(k\,t^*)\| - \|\mathbf{x}(0)\|}{\|\mathbf{x}(0)\|} \right| \tag{5}$$

Using a 2-Dof and a 3-Dof Hamiltonians Zotos showed that, after a very short transition period of fluctuation, the *FNVI* displays a nearly constant value for regular orbits, while it continues to fluctuate significantly for chaotic orbits [18]. It results a qualitative indicator regarding the nature of an orbit. Zotos proceeded one step further by introducing a quantitative criterion. He calculated for every orbit the maximum and minimum value of *FNVI* when $t \in [200\,s, 1000\,s]$ and defined

$$dFNVI = FNVI_{\max} - FNVI_{\min} \tag{6}$$

He proposed as a threshold value between regularity and chaoticity the value 0.05 so when $dFNVI > 0.05$ the orbit is chaotic, while when $dFNVI \le 0.05$ the orbit is ordered.

3 HAMILTON'S EQUATIONS OF MOTION FOR THE DOUBLE PENDULUM

The double pendulum is one of the simplest examples of a time-independent Hamiltonian system that exhibits chaotic behavior. It is one simple pendulum fixed to the end of another simple pendulum as shown in Figure 1. The top and center pivots are assumed frictionless, and the coupled objects are free to rotate about them in the vertical plane under the action of gravity. The upper pendulum is modeled as a massless rod of length l_1 with a bob of mass m_1 on the end. The lower pendulum is attached to the mass of the upper pendulum and is similarly a massless rod of length l_2 and a bob of mass m_2.

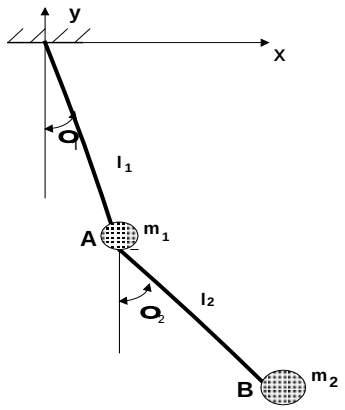

Figure 1: Double pendulum system

The double pendulum exhibits a rich behavior and provides a convenient demonstration of nonlinear dynamics and chaos [19, 20]. Its equations of motion may be derived using Hamiltonian dynamics. To do this, let consider the positions (x_1, y_1) and (x_2, y_2) of the bobs at a given instant of time

$$\begin{aligned} x_1 &= l_1 \sin\theta_1 \quad , \quad y_1 = -l_1 \cos\theta_1 \\ x_2 &= l_1 \sin\theta_1 + l_2 \sin\theta_2 \quad , \quad y_2 = -l_1 \cos\theta_1 - l_2 \cos\theta_2 \end{aligned} \tag{7}$$

Therefore, there are only two independent generalized coordinates, which can be taken to be the angles θ_1 and θ_2 that the two rods make with downward vertical direction. The kinetic (T) and potential (V) energies of the system are given by

$$T = \frac{1}{2} m_1 \left(\dot{x}_1^2 + \dot{y}_1^2 \right) + \frac{1}{2} m_2 \left(\dot{x}_2^2 + \dot{y}_2^2 \right) \quad , \quad V = m_1 g y_1 + m_2 g y_2 \tag{8}$$

where *g* is the constant gravitational acceleration and dots denote the derivatives with respect to time. The Lagrangean relates the kinetic and potential energies of the system. It is described as

$$\begin{aligned} L\left(\theta_1, \theta_2, \dot{\theta}_1, \dot{\theta}_2 \right) &= T - V = \frac{1}{2}(m_1 + m_2) l_1^2 \dot{\theta}_1^2 + \frac{1}{2} m_2 l_2^2 \dot{\theta}_2^2 + m_2 l_1 l_2 \dot{\theta}_1 \dot{\theta}_2 \cos(\theta_1 - \theta_2) + \\ &+ (m_1 + m_2) g l_1 \cos\theta_1 + m_2 g l_2 \cos\theta_2 \end{aligned} \tag{9}$$

The generalized moments p_1 and p_2 can be found from the Lagrangean as follows

$$p_1 = \frac{\partial L}{\partial \dot{\theta}_1} = (m_1 + m_2) l_1^2 \dot{\theta}_1 + m_2 l_1 l_2 \dot{\theta}_2 \cos(\theta_1 - \theta_2)$$
$$p_2 = \frac{\partial L}{\partial \dot{\theta}_2} = m_2 l_2^2 \dot{\theta}_2 + m_1 l_1 l_2 \dot{\theta}_1 \cos(\theta_1 - \theta_2) \tag{10}$$

From (4), the angular velocities $\dot{\theta}_1$ and $\dot{\theta}_2$ can be expressed as functions of the coordinates and moments

$$\dot{\theta}_1 = \frac{l_2 p_1 - l_1 p_2 \cos(\theta_1 - \theta_2)}{l_1^2 l_2 \left[m_1 + m_2 \sin^2(\theta_1 - \theta_2)\right]} \quad , \quad \dot{\theta}_2 = \frac{l_1 (m_1 + m_2) p_2 - l_2 m_2 p_1 \cos(\theta_1 - \theta_2)}{l_2^2 l_1 m_2 \left[m_1 + m_2 \sin^2(\theta_1 - \theta_2)\right]} \tag{11}$$

The Hamiltonian H is the Legendre transform of the Lagrangean L

$$H\left(\theta_1, \theta_2, \dot{\theta}_1, \dot{\theta}_2\right) = \dot{\theta}_1 p_1 + \dot{\theta}_2 p_2 - L = -(m_1 + m_2) g l_1 \cos\theta_1 - m_2 g l_2 \cos\theta_2 +$$
$$+ \frac{m_2 l_2^2 p_1^2 + (m_1 + m_2) l_1^2 p_2^2 - 2 m_2 l_1 l_2 p_1 p_2 \cos(\theta_1 - \theta_2)}{2 l_1^2 l_2^2 m_2 \left[m_1 + m_2 \sin^2(\theta_1 - \theta_2)\right]} \tag{12}$$

Hamilton's equations for the time rate of change of the generalized moments are

$$\dot{p}_1 = -\frac{\partial H}{\partial \theta_1} = C_2 - C_1 - (m_1 + m_2) g l_1 \sin\theta_1$$
$$\dot{p}_2 = -\frac{\partial H}{\partial \theta_2} = C_1 - C_2 - m_2 g l_2 \sin\theta_2 \tag{13}$$

where

$$K = \frac{m_2 l_2^2 p_1^2 + (m_1 + m_2) l_1^2 p_2^2 - 2 m_2 l_1 l_2 p_1 p_2 \cos(\theta_1 - \theta_2)}{2 l_1^2 l_2^2 m_2 \left[m_1 + m_2 \sin^2(\theta_1 - \theta_2)\right]}$$
$$C_1 = \frac{p_1 p_2 \sin(\theta_1 - \theta_2)}{l_1 l_2 \left[m_1 + m_2 \sin^2(\theta_1 - \theta_2)\right]}, \; C_2 = \frac{m_2 K \sin 2(\theta_1 - \theta_2)}{m_1 + m_2 \sin^2(\theta_1 - \theta_2)} \tag{14}$$

The set of the four equations (5) and (13) describe the time evolution of any orbit in the four-dimensional phase - space $(\theta_1, \theta_2, p_1, p_2)$. Because the Hamiltonian is conserved in time, the orbits actually lie on a three-dimensional hyper-surface determined by the equation

$$E = H + g\left[(m_1 + m_2) l_1 + m_2 l_2\right] = \text{constant} \tag{15}$$

The constant $(m_1 + m_2) l_1 + m_2 l_2$ has been added to H so $E = 0$ at the stable equilibrium point $\theta_1 = \theta_2 = p_1 = p_2 = 0$ [21, 22].

4 NUMERICAL RESULTS AND DISCUSSION

To investigate the detailed dynamics of the double pendulum the equations of motion are solved numerically by using the Mat Lab's solver ODE 45. For the simulation assume that the two masses are equal to unity, $m_1 = m_2 = 1kg$, and that the two lengths are also equal to unity, $l_1 = l_2 = 1m$. The equation (15) reduce to

$$E=\frac{p_1^2+2p_2^2-2p_1p_2\cos(\theta_1-\theta_2)}{1+\sin^2(\theta_1-\theta_2)}+g(3-2\cos\theta_1-\cos\theta_2)=\text{constant} \tag{16}$$

The accuracy of the integration may be checked by evaluating the energy of the pendulum at each integration step. Figure 2 shows the results for the four values of energy we will consider in the next simulations, namely $E_1=5J$, $E_2=10J$, $E_3=15J$ and $E_4=20J$. An obvious conservation of energy is easy to observe.

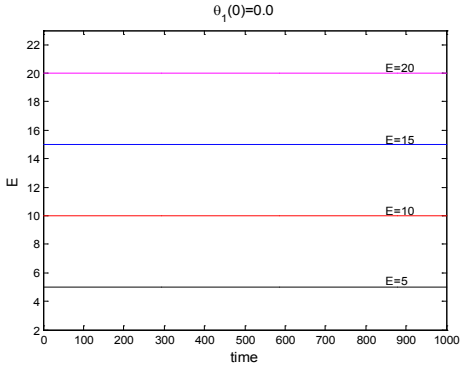

Figure 2: Conservation of the total energy E during the integration process

In order to illustrate the behavior of the FNVI in the case of the double pendulum system we consider two representative orbits. The first is an ordered orbit with initial condition $(\theta_1,\theta_2,p_1,p_2)=(1.1,0.0,0.0,2.7746)$ and the second is a chaotic orbit with initial conditions $(\theta_1,\theta_2,p_1,p_2)=(0.0,0.0,0.0,3.873)$. For both orbits, the value of energy is $E_3=15J$. The motion of the outer bob is depicted in Figure 3.

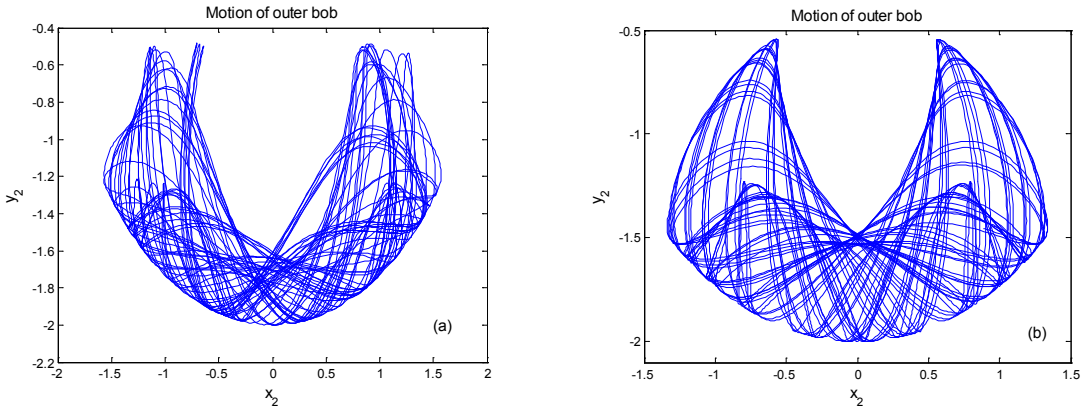

Figure 3: The motion of the outer bob: a) chaotic orbit; b) ordered orbit

When other two orbits are launched at a distance of 0.001 from these initial conditions, the orbits corresponding to the ordered case move practically together (indicating that there is no divergence of the two close orbits) while the orbits corresponding to the chaotic case move away from each other after a short time period, as shown in Figure 4.

Figure 5a presents the Poincare section of surface (*PSS*) of the two orbits defined by $\theta_2=0, p_2\geq 0$. The points of the ordered orbit (red points) form a set of smooth closed curves while the points of the chaotic orbit (black points) appear randomly scattered. Finally, in Figure 5b we plot the evolution in time of log(*SALI*) for the two orbits. The *SALI* of the ordered

orbit (grey points) fluctuates around *SALI* = 0.38, indicating the regular character of the orbit, while the *SALI* of the chaotic orbit (black points) falls abruptly reaching the limit of the accuracy of the computer precision after about 500 time units. All the logarithms in the paper are taken in base 10.

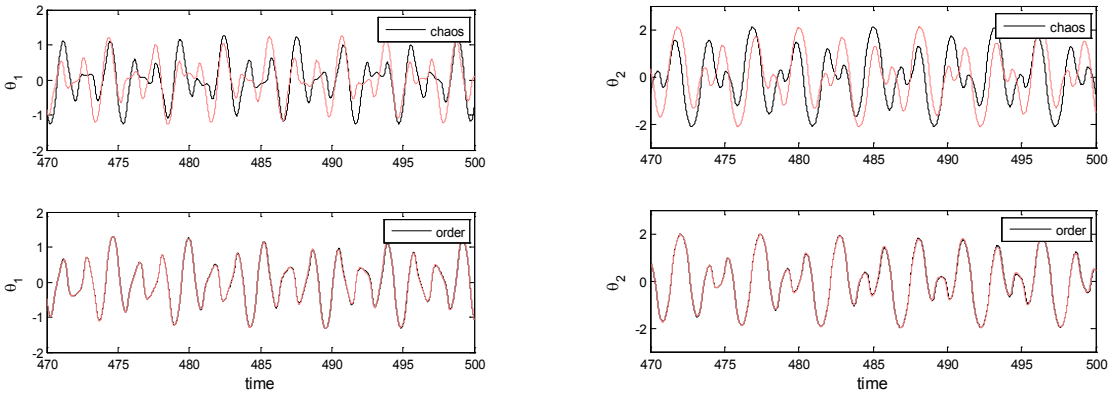

Figure 4: The time evolution of $\theta_1(t)$ and $\theta_2(t)$ for two very closed initial conditions in chaotic case (upper panels) and ordered case (lower panels)

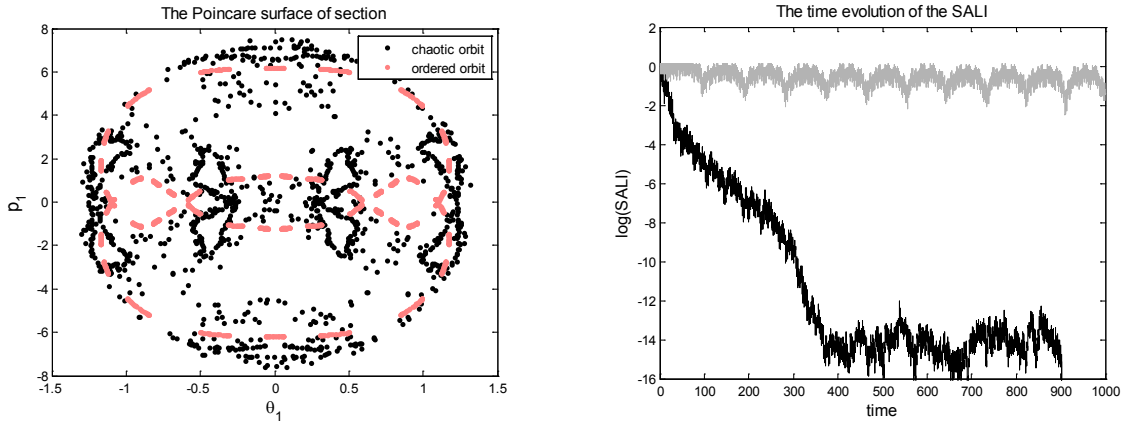

Figure 5: a) The PSS of the ordered orbit (red points) and chaotic orbit (black points); b) The time evolution of the log(*SALI*) for ordered orbit (grey points) and chaotic orbit (black points)

A short inspection of definition (5) shows a double dependence with t^* of *FNVI*. The same is valid for *dFNVI* . It is obvious that if the values of t^* increases the value of *dFNVI* decreases. In fact, a dependence of the form $dFNVI \propto 1/t^*$ may be considered. We think that a better choice for the *FNVI* could be

$$FNVI(t) = \frac{1}{k}\sum_{i=1}^{k}\left|\frac{\left\|\mathbf{x}\left(i\,t^*\right)\right\| - \left\|\mathbf{x}(0)\right\|}{\left\|\mathbf{x}(0)\right\|}\right| \tag{17}$$

In this way, *FNVI* presents only a weak relationship with t^*, as shown in Table 1. No matter which value of t^* was considered, an evident distinction between the *FNVI* plots for

the two orbits may be observed. *FNVI* displays large and random variations for the chaotic orbit while it remains almost constant for the regular one (see Figure 6a). We fixed $t^* = 0.05$ in the remainder of this paper. To see if these patterns remain unchanged if the total time of numerical integration increases, we computed the *FNVI* for the same orbits but for a time period of 5,000 time units (t.u). The obtained results are displayed in Figure 6b.

t^*		0.01	0.02	0.05	0.075	0.1	0.5
dFNVI obtained with (17)	Ordered orbit	0.002814	0.002815	0.002823	0.002826	0.003021	0.005507
	Chaotic orbit	0.043784	0.043783	0.043778	0.043831	0.043854	0.043292

Table 1: The dependence of *dFNVI* with t^* for the orbits discussed in Figure 5

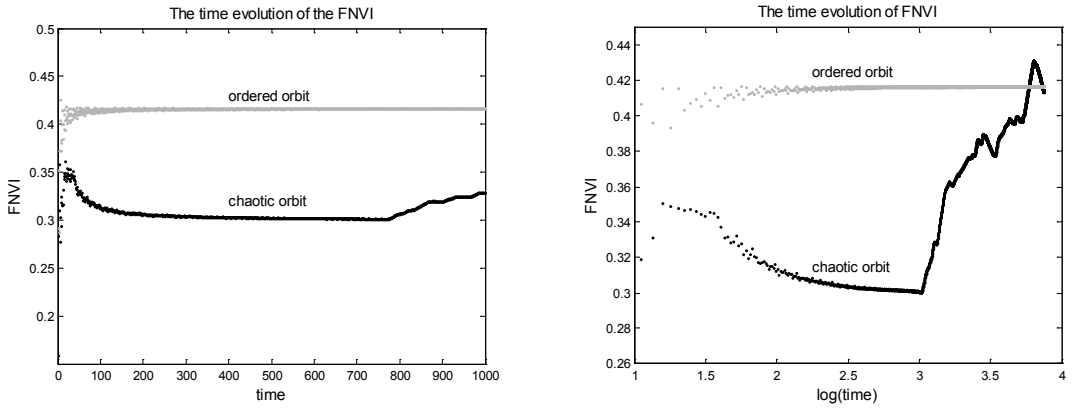

(a) (b)

Figure 6: The time evolution of the FNVI for ordered orbit (grey points) and chaotic orbit (black points): a) T=1,000; b) T= 5,000

It is interesting to mention that the *CPU* time needed to obtain the results plotted in Figure 5b it was fifty times greater than for results seen in Figure 6a. This might be a problem in the case of "sticky" orbits, which remain at the borders of an island of stability for a long time before enters the chaotic sea. The *PSS* technique and the *SALI* method, which require considerable *CPU* time, might give erroneous results if the running time is short enough.

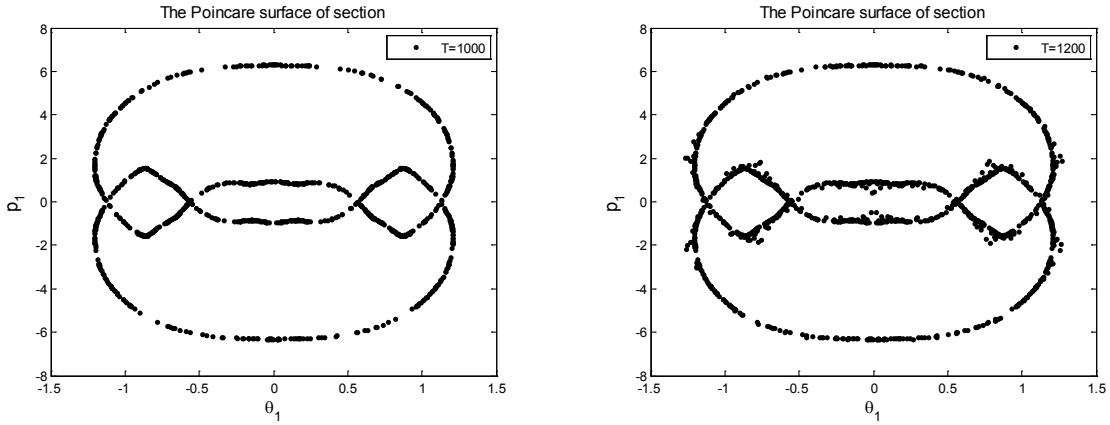

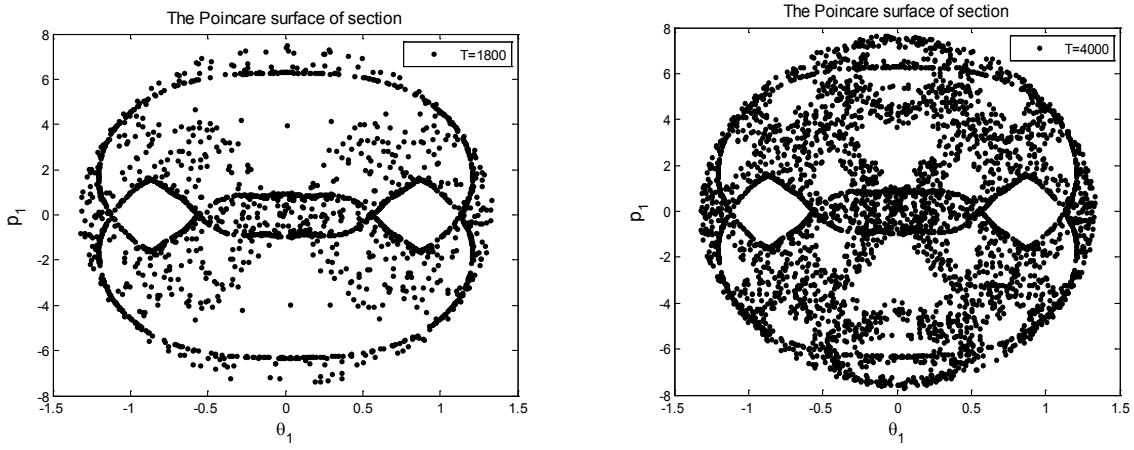

Figure 7: The PSS of the sticky orbit: a) T=1000; b) T=1200; c) T=1800; d) T=4000

To verify this, let consider the sticky orbit with initial conditions $(\theta_1, \theta_2, p_1, p_2) = (0.56525, 0.0, 0.0, 3.2174)$. Figure 7 shows the time evolution of the sticky orbit in the *PSS* (θ_1, p_1) for the integration times equal with T=1000 t.u., T=1200 t.u., T=1800 t.u. and T=4000 t.u. respectively. In the *PSS* corresponding to T=1000 t.u. the orbit seems to be regular. The first visible deviations from the smooth curve appear for T=1200 t.u. When T=4000 t.u. the orbit has left the borders of the island of stability and entered in the chaotic regime. Figure 8 presents the time evolution of the *FNVI* and the *SALI* for the same sticky orbit. The both figures indicate that after 1200 t.u. the orbit gradually alters its nature, from ordered to chaotic. The limit $SALI = 10^{-16}$ was obtained after T=2000 t.u. Although the conclusion is the same, the difference consists again in the *CPU* time.

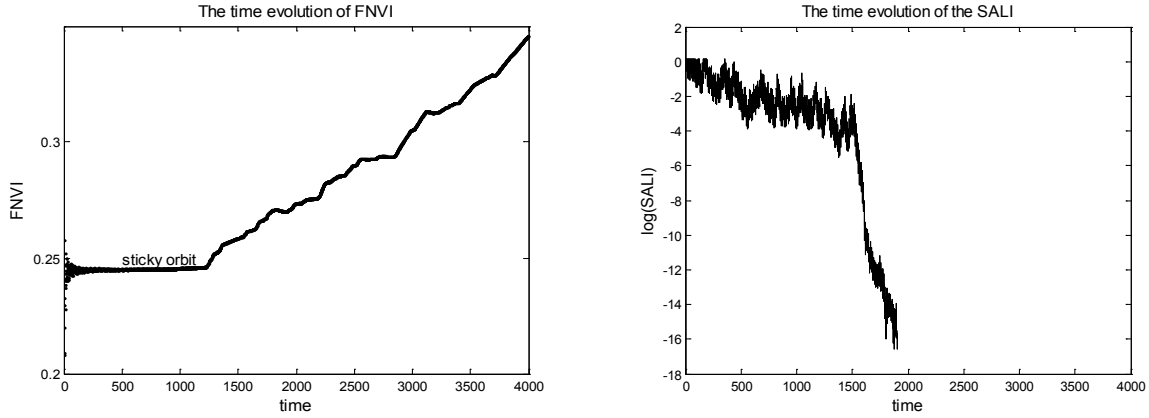

Figure 8: The time evolution of the *FNVI* (left panel) and of the *SALI* (right panel) for the sticky orbit discussed in Figure 7

In order to present the effectiveness of the *dFNVI* indicator in detecting regions of order and chaos we compute the *dFNVI* for a large grid of equally distributed initial conditions on the axis of the *PSS* (θ_1, p_1) of the double pendulum Hamiltonian. Firstly, in Figure 9 we present the *PSSs* of the system for $E_1 = 5J$, $E_2 = 10J$, $E_3 = 15J$ and $E_4 = 20J$. Each section was constructed by numerically solving Eqs. (5) and (13) for 40x40 initial conditions, chosen to provide a good coverage of the energetically accessible region in the plane. The appearance and growth of chaos with energy is well-demonstrated.

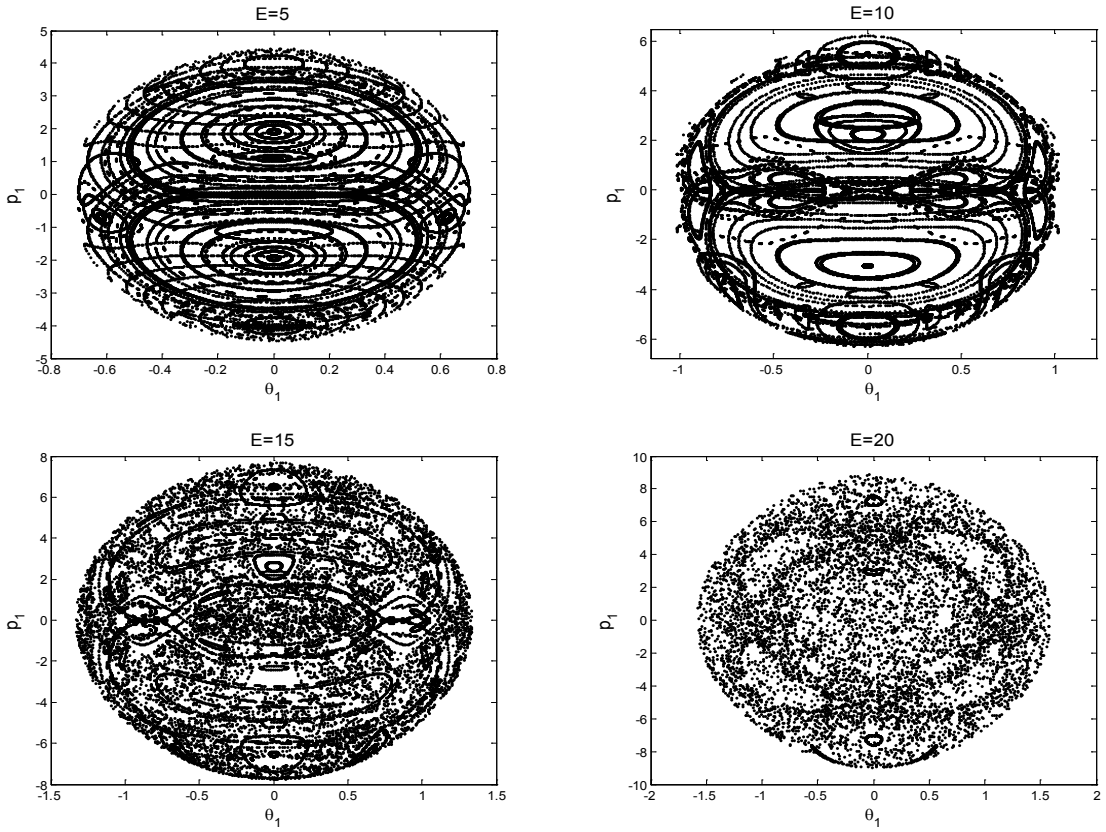

Figure 9:The *PSSs* of the double pendulum for increasing values of total energy *E*

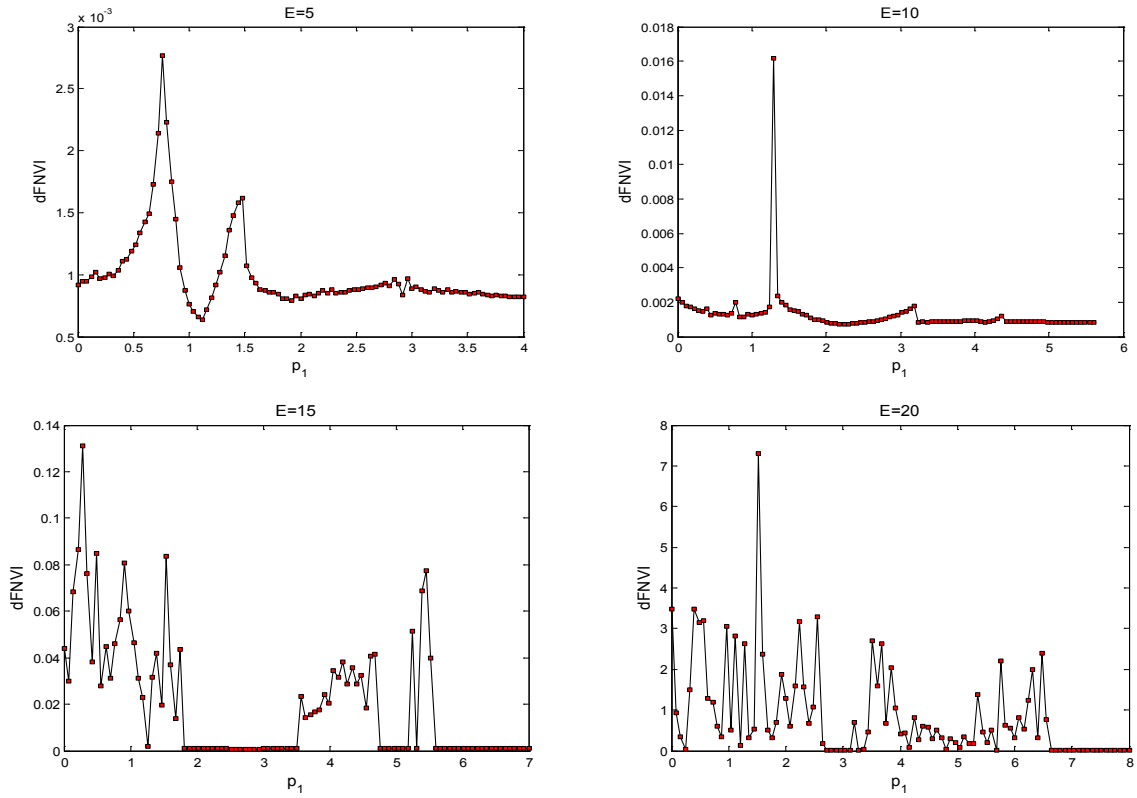

Figure 10: The variation of the *dFNVI* values for initial conditions chosen on the semi-line $\theta_1 = 0, p_1 \geq 0$ of the corresponding *PSS* of the double pendulum system

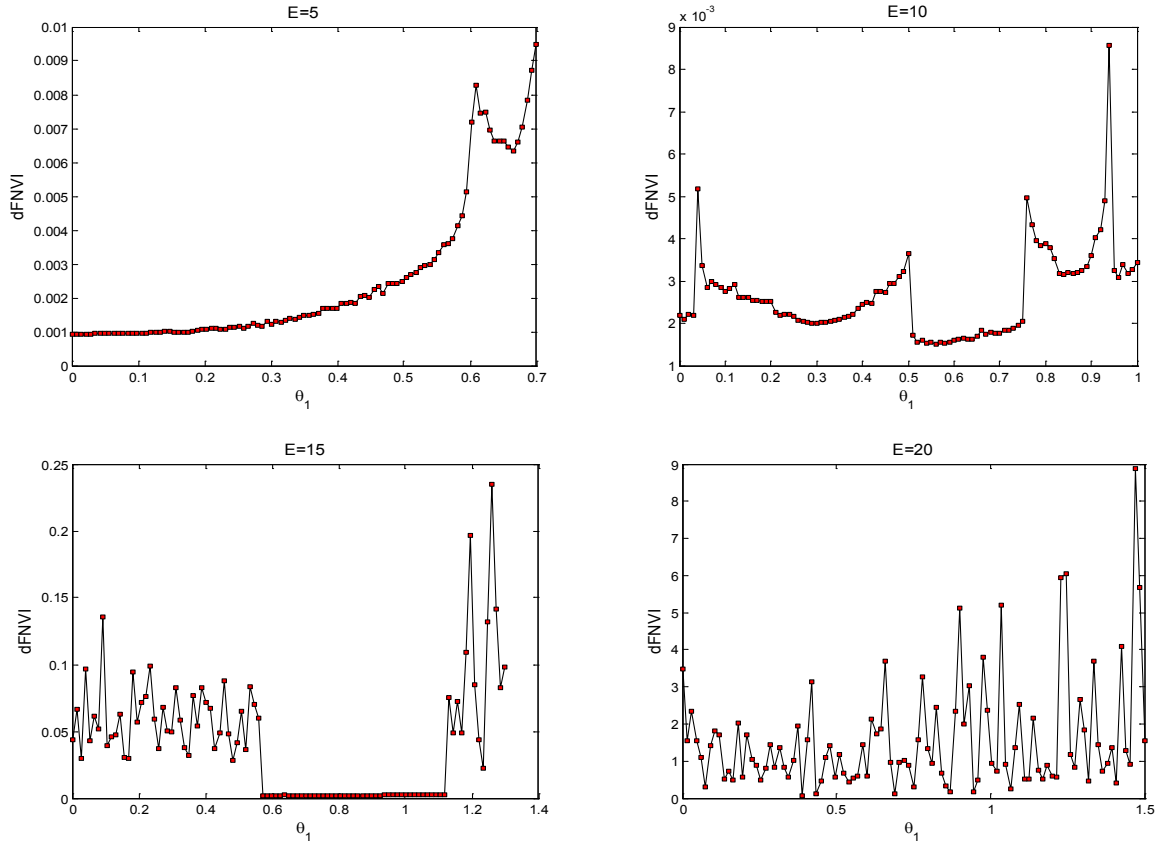

Figure 11: The variation of the *dFNVI* values for initial conditions chosen on the semi-line $p_1 = 0, \theta_1 \geq 0$ of the corresponding *PSS* of the double pendulum system

Secondly, in an attempt to define a threshold value between chaoticity and regularity we chose two sets of 100 equally distributed initial conditions on the semi-lines $\theta_1 = 0, p_1 \geq 0$ and $p_1 = 0, \theta_1 \geq 0$ of the *PSSs* depicted in Figure 9 and calculated their *dFNVI* values according with (6) and (17). The results are plotted in Figures 10 and 11. It is evident that as the value of the energy E increases, the values of the dFNVI increase too, especially for the chaotic orbits.

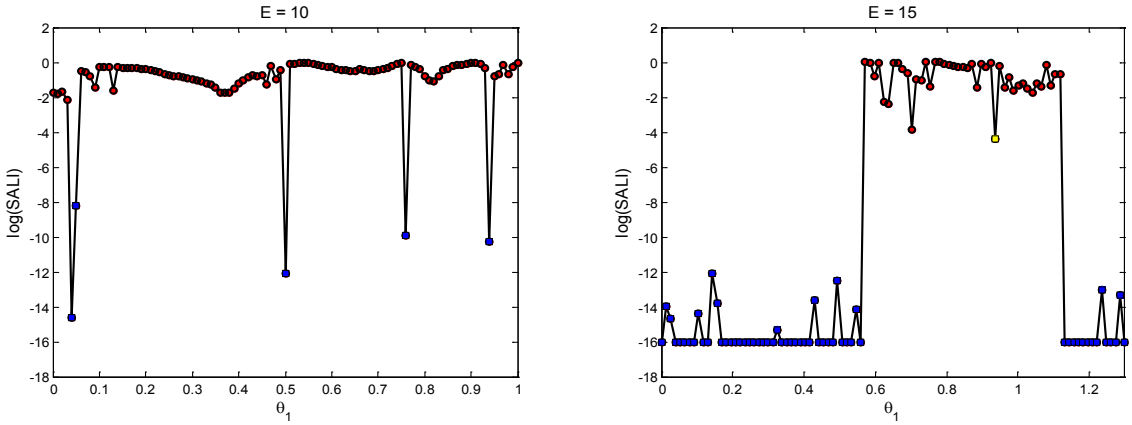

Figure 12: The variation of the *SALI* values for initial conditions chosen on the semi-line $p_1 = 0, \theta_1 \geq 0$ of the corresponding *PSS* of the double pendulum system

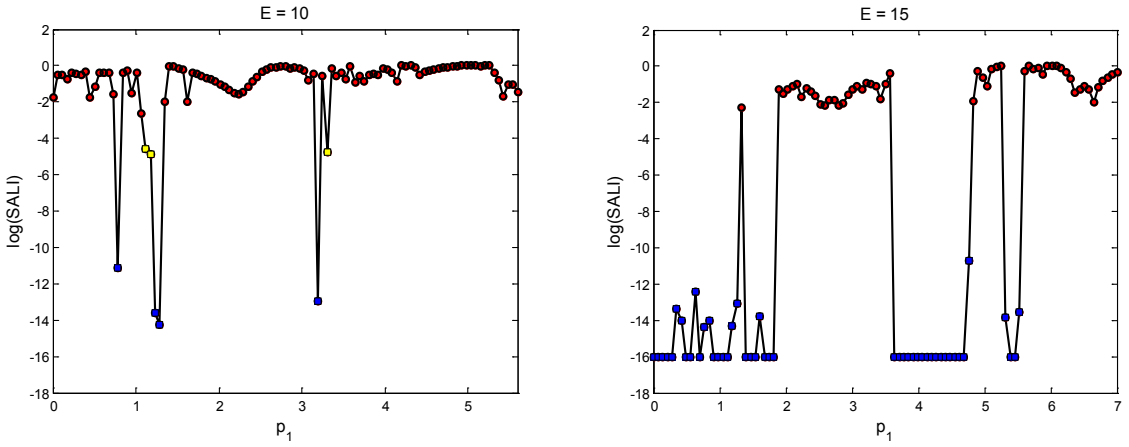

Figure 13: The variation of the *SALI* values for initial conditions chosen on the semi-line $\theta_1 = 0, p_1 \geq 0$ of the corresponding *PSS* of the double pendulum system

The same sets of initial conditions were used to compute the corresponding *SALI* values. The results are presented in Figures 12 and 13 only for $E_2 = 10J$ and $E_3 = 15J$. We assigned a coloured circle to every individual initial condition according to the *SALI's* value: if it is smaller than 10^{-8} the circle is coloured bleu (the orbit is chaotic beyond any doubt). If $SALI \in \left[10^{-8}, 10^{-4}\right)$ the circle is coloured yellow and finally, if $SALI \in \left[10^{-4}, 2\right)$ it is coloured red. Comparing Figures 10 and 13 and Figures 11 and 12 an obvious similitude between them is easy to observe. In fact, every orbit with $dFNVI \geq 0.01$ has $SALI \leq 10^{-8}$ therefore it is chaotic and almost all orbits having $dFNVI < 0.005$ are characterized by $SALI > 10^{-2}$ therefore they are ordered or "sticky" (with only three exceptions). None orbit has $dFNVI \in \left[0.005, 0.01\right]$.

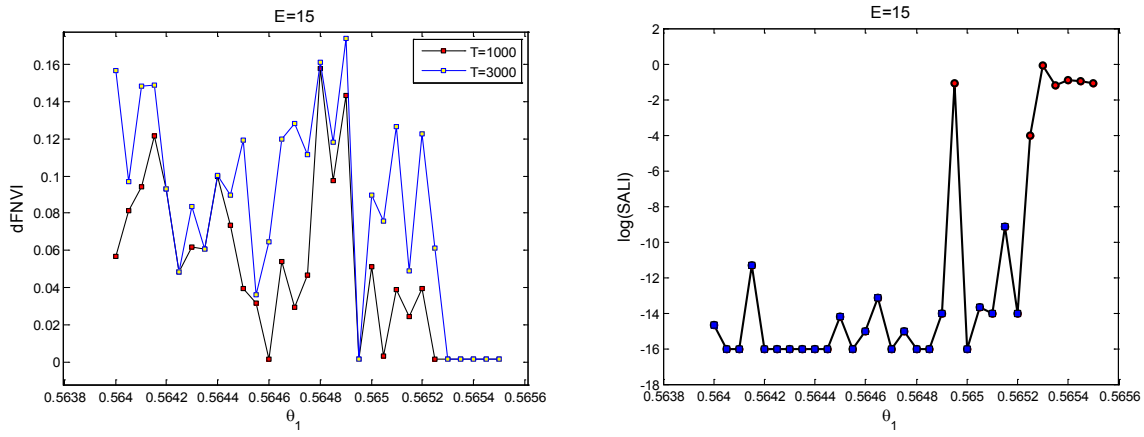

Figure 14: The variation of the *dFNVI* values (left panel) and *SALI* values (right panel) for initial conditions chosen on the interval $\theta_1 \in \left[0.564, 0.5655\right]$

Based on these numerical simulations, we propose as a threshold value between regularity and chaos the value 0.01. Thus when $dFNVI \geq 0.01$ the orbit is chaotic while when $dFNVI < 0.01$ it is ordered.

In order to clear up the exceptions mentioned above, we carried out a carefully analysis of the interval $\theta_1 \in \left[0.564, 0.5655\right]$, corresponding to the total energy $E_3 = 15J$ in Figure 12. This

zone hallmarks the passage from a region where the motion is chaotic to a huge island of stability and it is expecting that a significant number of sticky orbits could be detected in here. Figure 14 present our findings. In the left panel were displayed the *dFNVI* values calculated for T=1000 t.u. and T=3000 t.u. while in the right panel were depicted the associated *SALI* values, obtained with T=1000 t.u. Two remarks are in order. Firstly, a lot of *dFNVI* values increase when the definition (6) is extended to the interval [200s, 3000s]. In this category must be included three orbits which resemble ordered on the time interval [200s, 1000s], but which are in fact sticky orbits. Secondly, the *SALI* values always give the right verdict regarding the nature of he orbit. However, even if T=3000 t.u., the *CPU* time needed to obtain a *dFNVI* value remains smaller than for a *SALI* value.

5 CONCLUSIONS

In this paper we have illustrated the capacity of the Fast Norm Vector Indicator (*FNVI*) method in distinguishing between order and chaos in double pendulum system. For the sake of comparison, an accepted tool, the Smaller Alignment Index (*SALI*) was chosen. The main conclusions of the study can be summarized as follows:

- The *FNVI* seems to be a fast and accurate qualitative tool in order to determine if an orbit is ordered or chaotic. The distinction between these two types of orbits is based on the different behavior of the *FNVI*. It was found to fluctuate significantly for chaotic orbits, while displays a nearly constant value for ordered orbits.
- An important advantage of the *FNVI* method over the *SALI* method is the short *CPU* time needed to provide a conclusive result regarding the character of he orbit. This is because the *FNVI* method requires only the computation of the set of equations of motion while the *SALI* method needs the computation of the variational equations too. The *CPU* time on a Intel (R) Corel (TM) 2 Duo CPU T 5450 2.33 GHz, needed to obtain a conclusion, for an integration time of 1000 units of time, was about 12 sec/orbit with *FNVI* method and about 200 sec/orbit with *SALI* method. The *CPU* time could be a crucial criterion when we need o study a large number of orbits or when we follow the time evolution of a sticky orbit.
- The quantified version of the *FNVI*, the *dFNVI*, depends on the predefined time step t^* of the numerical integration. The proposed threshold value of 0.05 between order and chaos is valid, in our opinion, only for a particular t^*. An independent value of 0.01 could be considered instead, if the modified definition (17) of the *FNVI* is utilized.
- Exploiting the advantages of the *dFNVI* indicator, we have constructed detailed grid-plots where the chaotic and ordered regions are clearly distinguished. These grid-plots were plotted for increasing values of the total energy and were compared with the results supplied by the *SALI* method.
- Because the *dFNVI* was defined for the time interval [200s, 1000s] it is unable to distinguish between ordered and sticky orbits. For both types of orbits we found *dFNVI* < 0.005. This is because the sticky orbit, which is chaotic, need more time to escape from the outer region of an island of stability to the surrounding chaotic region. The *FNVI* plots, extended on a larger time interval, make the correct distinction between the two types of orbit.

REFERENCES

[1] G.L. Baker, J.P. Gollub, *Chaotic Dynamics: An Introduction*, Cambridge University Press, New York, 1990.

[2] G. Benettin, C. Froeschle, J.P. Scheidecker, Kolmogorov entropy of a dynamical system with an increasing number of degrees of freedom, *Phys. Rev. A* **19**, 2454-2460, 1979.

[3] R.L. Delaney, *An introduction to chaotic dynamical systems,* Addison-Wesley Publishing Company, New York, 1989.

[4] A. Wolfe, B. Swift, H.L. Swenney, J.A. Vastano, Determining Lyapunov exponents from a time series, *Physica D* **16**, 285-317, 1985.

[5] C. Froeschle, E. Lega, R. Gonczi, Fast Lyapunov Indicator. Application to asteroidal motion, *Celest. Mech. Dyn. Astron*., **67**, 41-62, 1997.

[6] L.M. Saha, R. Tehri, Application of recent indicators of regularity and chaos to discrete maps, *Int. J. of Appl. Math. and Mech*., **6**, 86-93, 2010.

[7] D. Deleanu, New applications of Fast Lyapunov Indicator for discrete-time dynamical systems, *Constanta Maritime University Annals*, **13**, 113-120, 2011.

[8] M. Fouchard, E. Lega, Ch. Froeschle, C.I. Froeschle, On the relationship between Fast Lyapunov Indicator and periodic orbits for continuous flows, *Celest. Mech. Dyn. Astron.*, **83**, 205-222, 2002.

[9] Ch. Skokos, Alignment indices: a new, simple method for determining the ordered or chaotic nature of orbits, *J. Phys. A: Math. Gen.*, **34**, 10029-10043, 2001.

[10] Ch. Skokos, T. Bountis, Ch. Antonopoulos, Geometrical properties of local dynamics in Hamiltonian systems: the Generalized Alignment Index method, *Physica D.*, **231**, 30-54, 2008.

[11] L.M. Saha, M. Budhraja, The largest eigenvalue: An indicator of chaos?, *Int. J. of Appl. Math. and Mech.*, **3(1)**, 61-71, 2007.

[12] D. Deleanu, Dynamic Lyapunov Indicator: a practical tool for distinguishing between ordered and chaotic orbits in discrete dynamical systems, *Proceedings of the 10th WSEAS International Conference on Non-Linear Analysis, Non-Linear Systems and Chaos (NOLASC' 11),* Iasi, Romania, July 1-3, 2011.

[13] N. Voglis, G. Contopoulos, C. Efthymiopoulos, Detecting of ordered and chaotic motion using the dynamical spectra, *Celest. Mech. Dyn. Astron.*, **73**, 211-220, 1999.

[14] Z. Sandor, B. Erdi, A. Szell, B. Funk, The Relative Lyapunov Indicator: an efficient method of chaos detection, *Celest. Mech. Dyn. Astron*., **90**, 127-138, 2004.

[15] G.A. Gottwald, I.A. Melbourne, A new test for chaos in deterministic systems, *Proc. Roy. Soc. London*, **460**, 603-611, 2004.

[16] P. Waz, D.D. Waz, Assymetry coefficients as indicators of chaos, *Acta Physica Polonica*, **116**, 987-991, 2009.

[17] G. Contopoulos, N. Voglis, Spectra of stretching numbers and helicity angles in dynamical systems, *Celest. Mech. Dyn. Astron*., **14**, 1-20, 1996.

[18] E.E. Zotos, The Fast Norm Vector Indicator method: a new dynamical parameter for detecting order and chaos in Hamiltonian systems, *Nonlinear Dyn.,* DOI 10.1007/s1107-012-0504-1.

[19] T. Shinbrot, C. Grebogi, J. Wisdom, J.A. Yorke, Chaos in a double pendulum, *Am. J. Phys*., **60**, 491-499, 1992.

[20] R.B. Levien, S.M. Tan, Double pendulum: an experiment in chaos, *Am. J. Phys.*, **61**, 1038-1044, 1993.

[21] T. Stachowiak, T. Okad, A numerical analysis of chaos in the double pendulum, *Chaos, Solitons and Fractals*, **29**, 417-422, 2006.

[22] Z. Zhou, C. Whiteman, Motions of double pendulum, *Nonlinear Analysis, Theory, Method and Applications*, **26**, 1177-1191, 1996.